Pergamon

Int. J. Solids Structures Vol. 35, Nos. 3–4, pp. 269–283, 1998

0020-7683/98 $19.00 + .00

PII: S0020-7683(97)00076-0

PONDING ON CIRCULAR MEMBRANES

CHRISTOPHER Y. TUAN
Department of Civil Engineering, University of Nebraska-Lincoln, Rm 125C Engineering Building, 60th and Dodge, Omaha, NE 68182-0178, U.S.A.

(*Received* 20 *March* 1996; *in revised form* 17 *February* 1997)

Abstract—Nonlinear circular membrane responses under partial and full ponding loads have been solved by the fourth-order Runge-Kutta numerical integration and by finite element simulation with good accuracy. Under partial ponding loads, a discontinuity exists in the curvature of the deformed membrane at the fluid boundary while an inflection point forms inside the ponding. An iterative finite element algorithm has also been developed for solving membrane ponding problems where inelastic material response becomes significant. The finite element simulation procedure was proven to be accurate when validated against test data from membrane forming experiments.

1. INTRODUCTION

Solutions for circular membranes under ponding loads are scarce in the literature, particularly when material response becomes inelastic. The load-deflection relation is strongly nonlinear in that the deformed shape of a membrane depends on the volume and distribution of the fluid, which, in turn, depends on the deformation. Practical implications include ponding on air-supported roofs (Szyszkowski and Glockner 1984), floating caps of oil storage tanks (Epstein 1980; Epstein and Strnad 1985), and optical reflector forming using ponding loads (Tuan and White 1990).

This paper focuses on large deformations and strains of initially flat, simply supported circular membranes under gradually accumulated fluid pressure due to ponding. Governing equations of elastic membranes under partial and full ponding loads were derived from variational energy considerations. The fourth-order Runge-Kutta numerical integration as well as an iterative finite element analysis using shell elements was conducted for elastic membrane response analysis. The same iterative finite element solution algorithm, validated against results from numerical integration, was also used for inelastic membrane response prediction of a forming experiment. Deformations and stresses of a stainless steel membrane under ponding loads were measured and the experimental data compared very closely with analytical results.

2. ELASTIC MEMBRANES UNDER PARTIAL AND FULL PONDING

It is of primary interest to determine the deformation and stresses in a membrane for a given volume of ponding fluid. Provided that the membrane is initially taut with negligible tension, the deflection of a point on the membrane after ponding has taken place can be resolved into a radial component $u(r)$ and a vertical component $w(r)$, as illustrated in Fig. 1.

The total potential energy of the system, Π, is composed of strain energy of the membrane, U_m, and potential drop of the ponding load, Ω:

$$\Pi = U_m + \Omega. \tag{1}$$

The elastic strain energy of a circular membrane can be expressed in terms of its radial and circumferential strains:

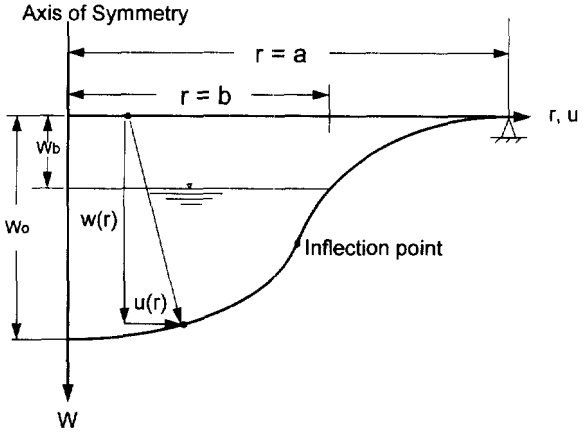

Fig. 1. Membrane deformation under ponding load.

$$U_m = \frac{\pi E t}{1-\nu^2}\int_0^a (\varepsilon_r^2 + \varepsilon_\theta^2 + 2\nu\varepsilon_r\varepsilon_\theta) r \, dr \tag{2}$$

where the Young's modulus, Poissons ratio, radius and thickness of the membrane are denoted by E, ν, a and t, respectively. The location of the fluid boundary is dictated by the volume of ponding, V:

$$V = 2\pi \int_0^b (w - w_b) r \, dr \tag{3}$$

where b is the radial distance to the fluid boundary, w_b is the vertical membrane displacement at $r = b$, and b must be in the range $0 \leqslant b \leqslant a$. The potential drop of the ponding load is

$$\Omega = -2\gamma\pi \int_0^b (w - w_b)\left[w_b + \frac{(w - w_b)}{2}\right] r \, dr \tag{4}$$

where γ is the unit weight of the fluid. The pressure distribution, $p(r)$, acting perpendicular to the deformed surface of the membrane, depends upon the location of the fluid boundary

$$p(r) = \gamma(w - w_b) \quad \text{for } 0 \leqslant r \leqslant b \tag{5}$$

$$p(r) = 0 \quad \text{for } b \leqslant r \leqslant a. \tag{6}$$

Based on the large deflection theory of plates (Timoshenko and Woinowsky, 1959), the strain-displacement relations for a circular membrane are

$$\varepsilon_r = \frac{du}{dr} + \frac{1}{2}\left(\frac{dw}{dr}\right)^2 \tag{7}$$

$$\varepsilon_\theta = \frac{u}{r}. \tag{8}$$

The stress-strain relations for elastic material response are

$$\sigma_r = \frac{E}{1-\nu^2}(\varepsilon_r + \nu\varepsilon_\theta) \tag{9}$$

$$\sigma_\theta = \frac{E}{1-\nu^2}(\varepsilon_\theta + \nu\varepsilon_r). \tag{10}$$

Substituting eqns (2), (4), (7) and (8) into eqn (1), the total potential energy of the system can be expressed in terms of membrane displacements as

$$\Pi = \frac{\pi Et}{1-\nu^2}\int_0^a \left\{\left[u' + \frac{1}{2}(w')^2\right]^2 + \left(\frac{u}{r}\right)^2 + 2\nu\left[u' + \frac{1}{2}(w')^2\right]\left(\frac{u}{r}\right)\right\} r\,\mathrm{d}r - \gamma\pi\int_0^b (w^2 - w_b^2) r\,\mathrm{d}r \tag{11}$$

where a prime denotes differentiation with respect to r. The variation in total potential energy, $\delta\Pi$ due to virtual displacements δu and δw is

$$\delta\Pi = \frac{\pi Et}{1-\nu^2}\int_0^a \left[2u'\delta u' + (w')^2\delta u' + 2u'w'\delta w' + (w')^3\delta w' + \frac{2u}{r^2}\delta u + \frac{2\nu u'}{r}\delta u + \frac{2\nu u}{r}\delta u' + \frac{\nu(w')^2}{r}\delta u + \frac{2\nu u w'}{r}\delta w'\right] r\,\mathrm{d}r - 2\gamma\pi\int_0^b (w - w_b)\delta w r\,\mathrm{d}r. \tag{12}$$

Integrating eqn (12) by parts gives:

$$\int_0^a 2u'\delta u' r\,\mathrm{d}r = 2ru'\delta u\Big|_0^a - \int_0^a 2(u' + ru'')\delta u\,\mathrm{d}r \tag{13}$$

$$\int_0^a (w')^2\delta u' r\,\mathrm{d}r = r(w')^2\delta u\Big|_0^a - \int_0^a [(w')^2 + 2rw'w'']\delta u\,\mathrm{d}r \tag{14}$$

$$\int_0^a 2vu\delta u'\,\mathrm{d}r = 2vu\delta u\Big|_0^a - \int_0^a 2vu'\delta u\,\mathrm{d}r \tag{15}$$

$$\int_0^a 2ru'w'\delta w'\,\mathrm{d}r = 2ru'w'\delta w\Big|_0^a - \int_0^a (2u'w' + 2ru''w' + 2ru'w'')\delta w\,\mathrm{d}r \tag{16}$$

$$\int_0^a r(w')^3\delta w'\,\mathrm{d}r = r(w')^3\delta w\Big|_0^a - \int_0^a [(w')^3 + 3r(w')^2w'']\delta w\,\mathrm{d}r \tag{17}$$

$$\int_0^a 2vuw'\delta w'\,\mathrm{d}r = 2vuw'\delta w\Big|_0^a - \int_0^a (2vu'w' + 2vuw'')\delta w\,\mathrm{d}r. \tag{18}$$

Forced boundary conditions require that $u = w' = 0$ at the membrane center ($r = 0$) and that $u = w = 0$ at the simple support ($r = a$). Therefore, δu and $w' = 0$ at $r = 0$ and δu and $\delta w = 0$ at $r = a$. The principle of minimum potential energy requires that $\delta\Pi = 0$ for any combinations of δu and δw, which are mutually independent, arbitrary virtual displacements compatible with the forced boundary conditions.

3. EQUATIONS OF EQUILIBRIUM

Grouping all the terms involving δu yields

$$\frac{\pi Et}{1-\nu^2}\int_0^a\left[2u'+2ru''+(1-\nu)(w')^2+2rw'w''-\frac{2u}{r}\right]\delta u\,\mathrm{d}r=0. \tag{19}$$

Since δu is arbitrary, the integrand in the brackets in eqn (19) must vanish. This integrand is the equilibrium equation in the radial direction. Using eqns (7)–(10), this equation of equilibrium can be expressed alternatively in terms of membrane stresses as

$$\sigma_r-\sigma_\theta+r\frac{\mathrm{d}\sigma_r}{\mathrm{d}r}=0. \tag{20}$$

Grouping all the terms involving δw yields

$$\int_0^b\left\{\frac{\pi Et}{1-\nu^2}\left[\frac{u'w'}{r}+u''w'+u'w''+\frac{(w')^3}{2r}+\frac{3}{2}(w')^2w''+\frac{\nu u'w'}{r}+\frac{\nu uw''}{r}\right]+\gamma\pi(w-w_b)\right\}\delta w r\,\mathrm{d}r=0. \tag{21}$$

Since δw is arbitrary, the integrand in the braces in eqn (21) must vanish. Note that this integrand is the equation of equilibrium for $0\leqslant r\leqslant b$ in the vertical direction which can be expressed alternatively as

$$\frac{\mathrm{d}\sigma_r}{\mathrm{d}r}\left(\frac{\mathrm{d}w}{\mathrm{d}r}\right)+\frac{\sigma_r}{r}\left(\frac{\mathrm{d}w}{\mathrm{d}r}\right)+\sigma_r\left(\frac{\mathrm{d}^2w}{\mathrm{d}r^2}\right)+\frac{\gamma}{t}(w-w_b)=0. \tag{22}$$

The equation of equilibrium for $b\leqslant r\leqslant a$ in the vertical direction is

$$\frac{\mathrm{d}\sigma_r}{\mathrm{d}r}\left(\frac{\mathrm{d}w}{\mathrm{d}r}\right)+\frac{\sigma_r}{r}\left(\frac{\mathrm{d}w}{\mathrm{d}r}\right)+\sigma_r\left(\frac{\mathrm{d}^2w}{\mathrm{d}r^2}\right)=0. \tag{23}$$

These equations of equilibrium must be satisfied whether the membrane material response is elastic or not.

4. NUMERICAL SOLUTION TO ELASTIC MEMBRANE RESPONSE

The finite elastic deformation of circular membranes under prescribed axisymmetric pressure loading has been studied extensively (e.g., Kao and Perrone, 1971; Kelkar *et al.*, 1985). However, an iterative algorithm must be included in the solution procedures for a ponding problem since the pressure loading is not known in advance.

4.1. *Membranes under full ponding loads*

Epstein and Strnad (1985) showed that eqns (20) and (22) can be reduced to two coupled nonlinear differential equations in terms of w and σ_r:

$$r^2\frac{d^2\sigma_r}{dr^2}+3r\frac{d\sigma_r}{dr}+\frac{E}{2}\left(\frac{dw}{dr}\right)^2=0 \tag{24}$$

$$\frac{d\sigma_r}{dr}\left(\frac{dw}{dr}\right)+\frac{\sigma_r}{r}\left(\frac{dw}{dr}\right)+\sigma_r\left(\frac{d^2w}{dr^2}\right)+\frac{\gamma}{t}w=0 \tag{25}$$

with the natural boundary conditions

$$\frac{d\sigma_r}{dr}=0 \quad \text{at } r=0 \tag{26}$$

and

$$\sigma_r(1-\nu)+r\left(\frac{d\sigma_r}{dr}\right)=0 \quad \text{at } r=a \tag{27}$$

provided that the membrane is under full ponding load and made of a Hookean material with Young's modulus E and Poisson's ratio ν. The vertical deflection w and radial stress σ_r of the membrane are first solved simultaneously by numerically integrating $d\sigma_r/dr$ and dw/dr in eqns (24) and (25) using the fourth-order Runge-Kutta method. Initial guesses of σ_r and w are required in order to propagate solutions from center of the membrane to the edge of the membrane. The circumferential stress σ_θ is next calculated from eqn (20), and the horizontal displacement u is calculated from eqn (8) once the circumferential strain ε_θ is determined from the stress-strain relations, i.e., eqns (9) and (10). The boundary conditions $u = w = 0$ and eqn (27) are used as checks at $r = a$.

4.2. *Membranes under partial ponding loads*

The numerical solution algorithm is modified slightly for membranes under partial ponding loads. An initial depth of ponding, $w^* = w - w_b$ at the membrane center is assumed at the beginning of the numerical integration for a given fluid boundary b. Then eqn (22) is integrated along with eqn (24) simultaneously until the fluid boundary ($r = b$) is reached. The true value of w^* should be zero at this point and eqn (23) is integrated along with eqn (24) from this point out to the support. The value thus obtained at the support ($r = a$) should be $w^* = -w_b$ and the deformed shape of the membrane can be recovered by $w = w^* + w_b$.

4.3. *Numerical example*

A simply supported circular membrane made of a stainless steel was subjected to hydrostatic ($\gamma = 9.8$ kN/m^3) ponding loads. Its geometric and material properties are given in Table 1. The membrane was loaded until the water boundary was at 25%, 50%, 75%, and 100% of the membrane radius, respectively. Numerical solutions to these load cases were obtained by using the fourth-order Runge-Kutta method with an integration step of

Table 1. Geometric and material properties of the test membrane

Physical parameters (1)	Data (2)
Membrane material	304 stainless steel
Membrane radius, a	1.857 m (73.1 in)
Membrane thickness, t	0.051 mm (0.002 in)
Young's modulus, E	208 GPa (30,000 ksi)
Poisson's ratio, ν	0.33
Yield stress, σ_y	240 MPa (34 ksi)
Yield strain, ε_y	0.00115
Ultimate stress, σ_u	476 MPa (68 ksi)
Ultimate strain, ε_u	0.08

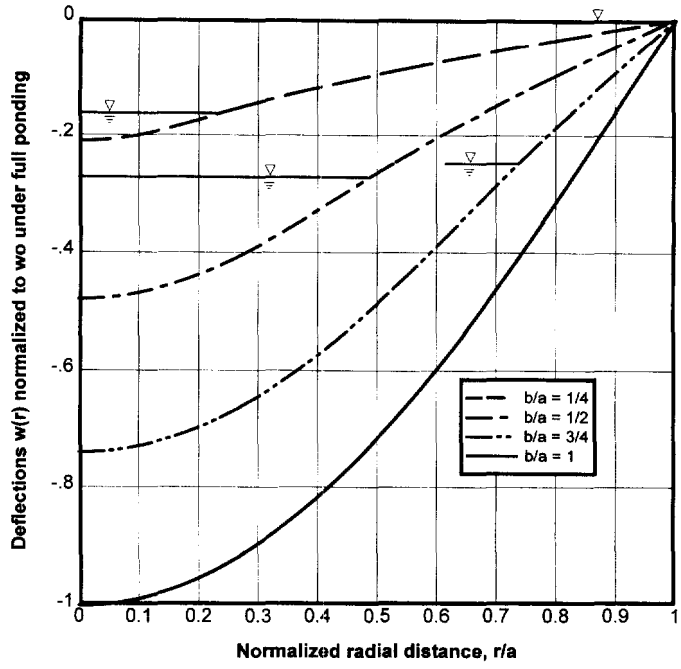

Fig. 2. Normalized membrane deformed shapes under various levels of ponding.

0.019 in (0.0483 cm). The deformed shapes (i.e., $r+u(r)$ vs $w(r)$) of the membrane are presented in Fig. 2, where the vertical deflections are normalized to the w_o when ponding was full. It was noted that the horizontal displacements were at least one order of magnitude smaller than the vertical deflections of the membrane, and thus their effects on the deformed shapes are insignificant. The horizontal displacement shapes are presented in Fig. 3, where the maximum displacement amplitudes were normalized to 1. Variations in the radial and

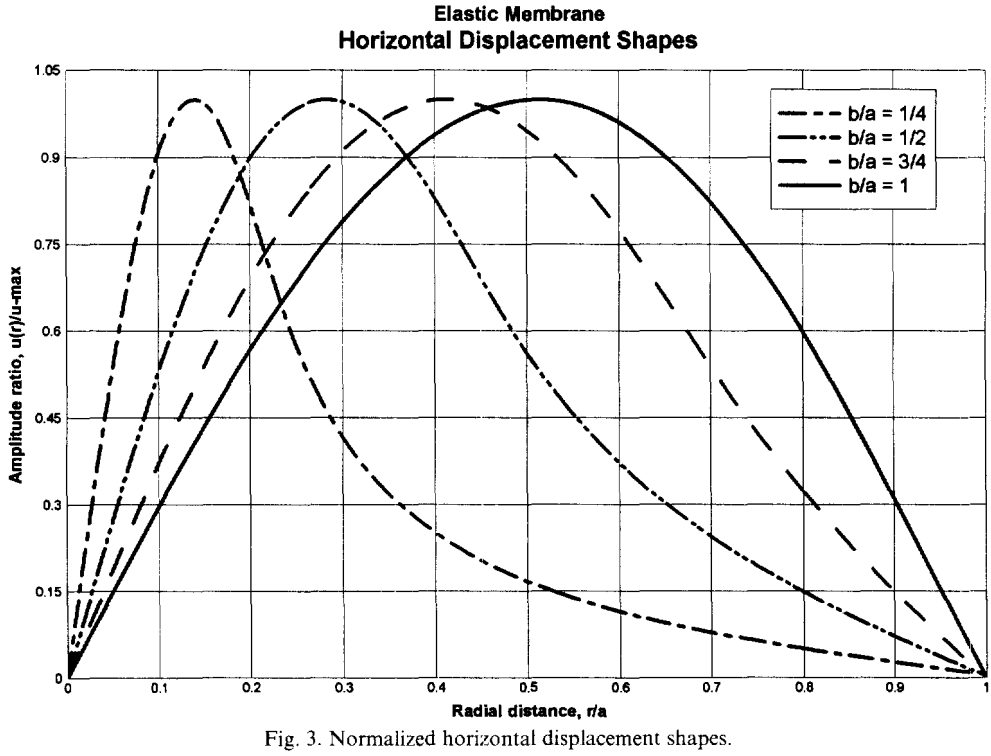

Fig. 3. Normalized horizontal displacement shapes.

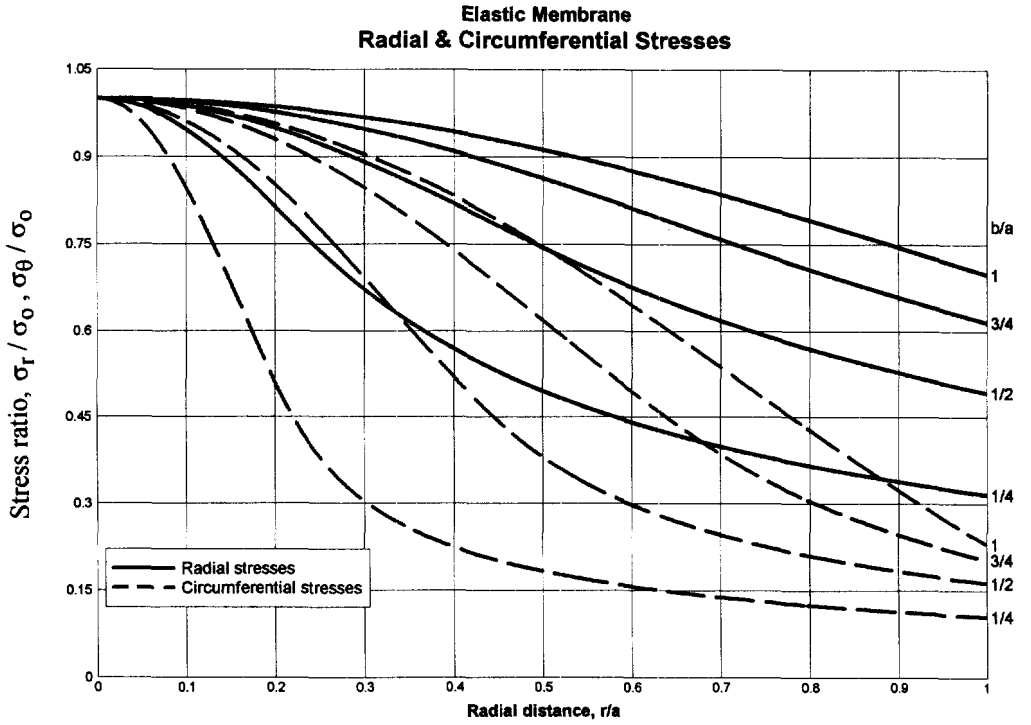

Fig. 4. Elastic membrane radial and circumferential stresses.

circumferential stresses along a radial line are depicted in Fig. 4. The curvature of the deformed membrane in the meridional direction can be expressed in terms of $u(r)$ and $w(r)$ as

$$\frac{1}{R} = \frac{1}{\left[\left(1+\frac{du}{dr}\right)^2 + \left(\frac{dw}{dr}\right)^2\right]^{3/2}}\left[-\frac{d^2w}{dr^2}\left(1+\frac{du}{dr}\right)+\frac{dw}{dr}\frac{d^2u}{dr^2}\right] \tag{28}$$

where R is the local radius of curvature. There is a discontinuity in the curvature at the fluid boundary (i.e., at $r = b$) where the slope remains continuous. In addition, an inflection point (curvature = 0) forms inside the ponding as shown in Fig. 5. These characteristics were also observed by Szyszkowski and Glockner (1984) in their investigation of the behavior of inflatable structures under ponding loads.

A finite element solution algorithm using ANSYS (Kohnke, 1993) code was developed to investigate the membrane deformations under ponding loads, for elastic membranes as well as for membranes where inelastic material behavior became significant. The membrane was modeled with 80 axisymmetric conical shell elements spanning from the center to the edge of the membrane. The shell elements were assigned the elastic material properties given in Table 1 for the membrane. The flowchart of this algorithm is shown in Fig. 6. The membrane response parameters obtained from the ANSYS simulations under partial to full ponding loads were virtually identical to those obtained by the fourth-order Runge-Kutta method and are presented in Table 2. Figure 7 provides a means to determine the maximum strain at membrane center and the radial distance to the water boundary for a given volume of ponding. The logic of the iterative finite element solution procedure was thus proven to be accurate by the independent solutions from direct numerical integration.

5. MEMBRANE FORMING EXPERIMENT WITH PONDING LOADS

Large reflector surfaces of high optical quality are attainable with the use of pressure-formed membranes. Among many alternate forming techniques, the "free-form yielding"

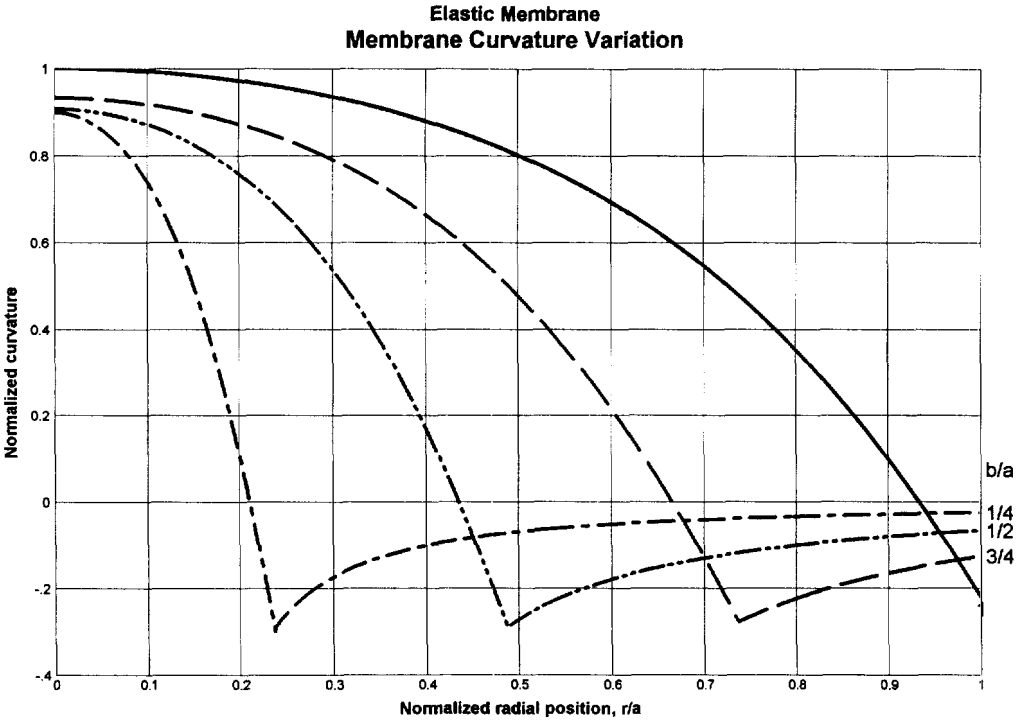

Fig. 5. Normalized membrane surface curvatures.

process, in which an initially flat membrane is plastically formed to a parabolic shape in the absence of a mold or mandrel, was successfully implemented by the engineering staff of Solar Kinetics, Inc., Dallas, Texas. The forming experiment provided the necessary data for the validation of the finite element simulation procedure developed to predict the inelastic response of a circular membrane under ponding loads.

5.1. *Forming experiment setup*

Test membranes were stretched over a 12 ft (3.71 m)-diameter steel cylinder, 14 in (0.36 m) tall and 0.75 in (19 mm) thick, before forming. The cylinder and its fitted flanges provided a rigid circumferential support for the test membranes. An initial parabolic shape with a center deflection of 0.965 in (2.45 cm) was first induced by slightly vacuuming the plenum behind the membrane. Next, the membrane was gradually loaded under the axisymmetric nonuniform pressure distribution due to water accumulation on the membrane surface as shown in Fig. 8(a). When the water level reached the membrane edge, the vacuum pressure was increased to induce additional ponding. This process was repeated until a desirable w_o was reached. A membrane surface was plastically formed after the fluid was gradually removed, also in an axisymmetric fashion, and a uniform stabilization pressure was applied to minimize the elastic rebound of the membrane. Membrane deflection and strain data were taken at the end of each successive loading when ponding was full. Membrane deflections at discrete points along a diametrical line was measured directly. The membrane slopes were calculated from the deflection data. Bi-directional strain gages were installed at the membrane center and the edge to measure the radial and circumferential strains at those locations. Figure 8(b) shows a plastically formed stainless steel membrane.

5.2. *Finite element simulation of the forming experiment*

A reliable model was required to predict the deformed membrane shapes in the forming experiments in order to determine the slope errors of formed surfaces from the desired parabolic shape. The iterative finite element solution scheme was used in the simulation of the membrane forming process under the gradual application of ponding load. The test

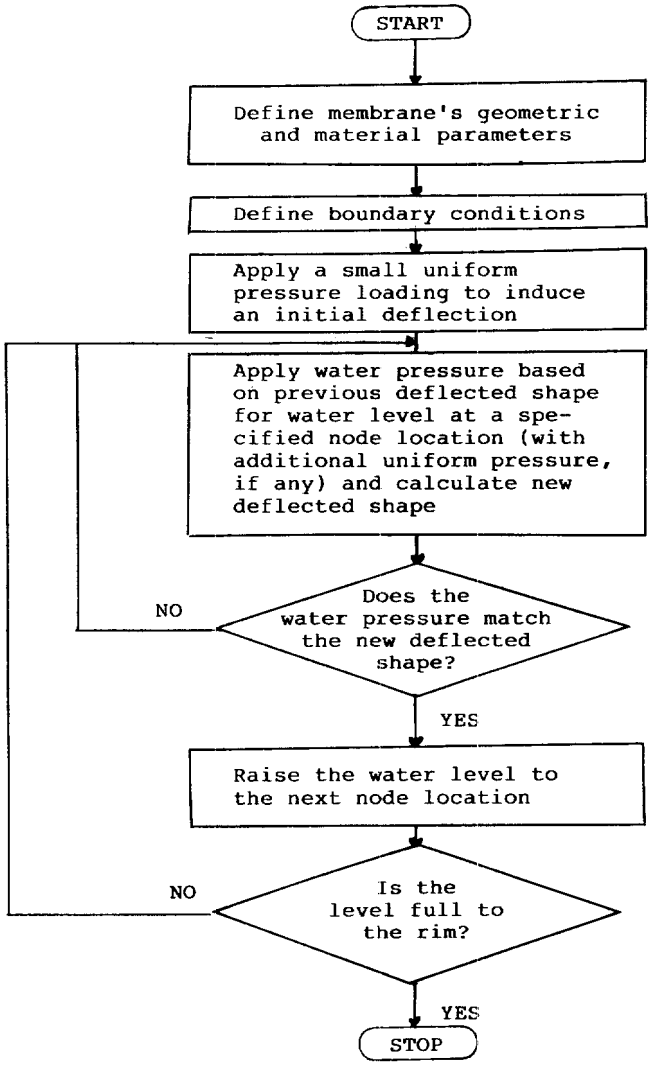

Fig. 6. Logic of the solution algorithm.

Table 2. Elastic membrane response under partial and full ponding loads

b (cm) (1)	w_o (cm) (2)	w_b (cm) (3)	V (cm^3) (4)	u_{max} (mm) (5)	$\sigma_o@r=0$ (MPa) (6)	$\sigma_r@r=a$ (MPa) (7)	$\sigma_\theta@r=a$ (MPa) (8)
20.89	0.42	0.37	30.36	0.000395	1.62	0.33	0.11
	(0.421)	(0.367)	(33.42)	(0.000427)	(1.702)	(0.333)	(0.110)
44.10	1.05	0.81	667.28	0.004	7.64	2.43	0.80
	(1.053)	(0.811)	(666.88)	(0.00404)	(7.647)	(2.429)	(0.802)
67.32	1.72	1.16	3635.0	0.014	17.84	7.40	2.44
	(1.724)	(1.158)	(3710.0)	(0.0143)	(17.850)	(7.399)	(2.445)
90.53	2.39	1.36	12236.0	0.035	32.36	16.02	5.30
	(2.397)	(1.364)	(11999.0)	(0.0347)	(32.366)	(16.020)	(5.301)
113.74	3.06	1.40	31012.0	0.0686	51.29	28.86	9.57
	(3.055)	(1.400)	(30390.0)	(0.0684)	(51.310)	(28.856)	(9.566)
136.95	3.70	1.24	66953.0	0.118	74.88	46.33	15.40
	(3.693)	(1.235)	(65595.0)	(0.1180)	(74.906)	(46.327)	(15.395)
160.17	4.31	0.82	130518.0	0.1862	103.55	68.78	22.94
	(4.313)	(0.826)	(127858.0)	(0.1856)	(103.577)	(68.779)	(22.937)
185.70	5.00	0.	253362.0	0.283	141.98	99.64	33.43
	(4.994)	(0.)	(253185.0)	(0.2824)	(142.02)	(99.645)	(33.428)

Note : The tabulated values were the results obtained by using the fourth-order Runge-Kutta numerical integration and ANSYS simulation results are shown in parentheses.

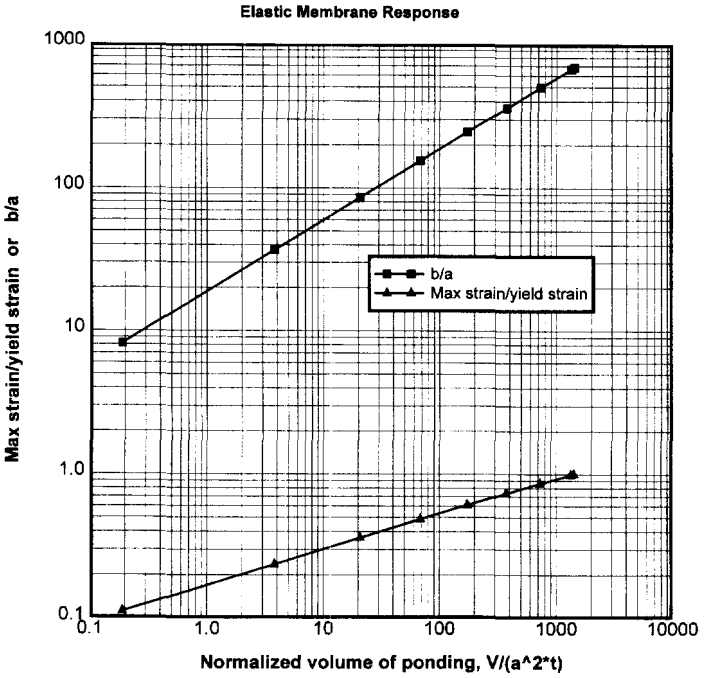

Fig. 7. Relation between ponding volume and maximum membrane strain.

membrane having the geometric and material properties given in Table 1 was modeled with 80 axisymmetic conical shell elements spanning from the center to the edge of the membrane. The stress-strain curve from a tension test of a 1-in. (2.54-cm) wide, 0.002-in (0.051-mm) thick strip of annealed, 304 stainless steel is shown in Fig. 9. The constitutive behavior of the 304 stainless steel was idealized as to follow the Prandtl-Reuss flow rule associated with the von Mises yield criterion (Mendelson, 1968). The stress stiffening effect due to membrane tension and the correction of load vectors for large deflections and rotations were also included in the finite element analysis. Since inelastic deformation is a load-path dependent process, the loading sequence in the forming experiment was closely followed in the finite element simulation. The numerical results are compared against the test data in Table 3. In load step No. 1, the initial membrane deflection induced by the vacuum resulted in additional ponding and produced a w_o about 20% more deflection under full ponding than the membrane center deflection obtained for an initially flat membrane. It was noted that all the predicted values compared very well with the experimental data except for the radial stresses measured at the membrane edge. The measured radial stresses at membrane edge appeared to be in error, since the ultimate tensile stress of 304 stainless steel is 68 ksi (476 MPa) at rupture.

The von Mises criterion predicts that yielding begins when the equivalent stress, σ_e, reaches the yield strength, σ_y. The equivalent stress is defined as

$$\sigma_e = \frac{1}{\sqrt{2}}[(\sigma_1-\sigma_2)^2+(\sigma_2-\sigma_3)^2+(\sigma_3-\sigma_1)^2]^{1/2} \tag{29}$$

where σ_1, σ_2, and σ_3 are the principal stresses. For a membrane, the equivalent stress is calculated as

$$\sigma_e^2 = \sigma_r^2 - \sigma_r\sigma_\theta + \sigma_\theta^2. \tag{30}$$

The variations of the equivalent stresses along a radial direction are shown in Fig. 10 for the load steps 4, 7 and 10. The membrane deflected shapes for these load steps normalized with respect to w_o in load step 1 are presented in Fig. 11.

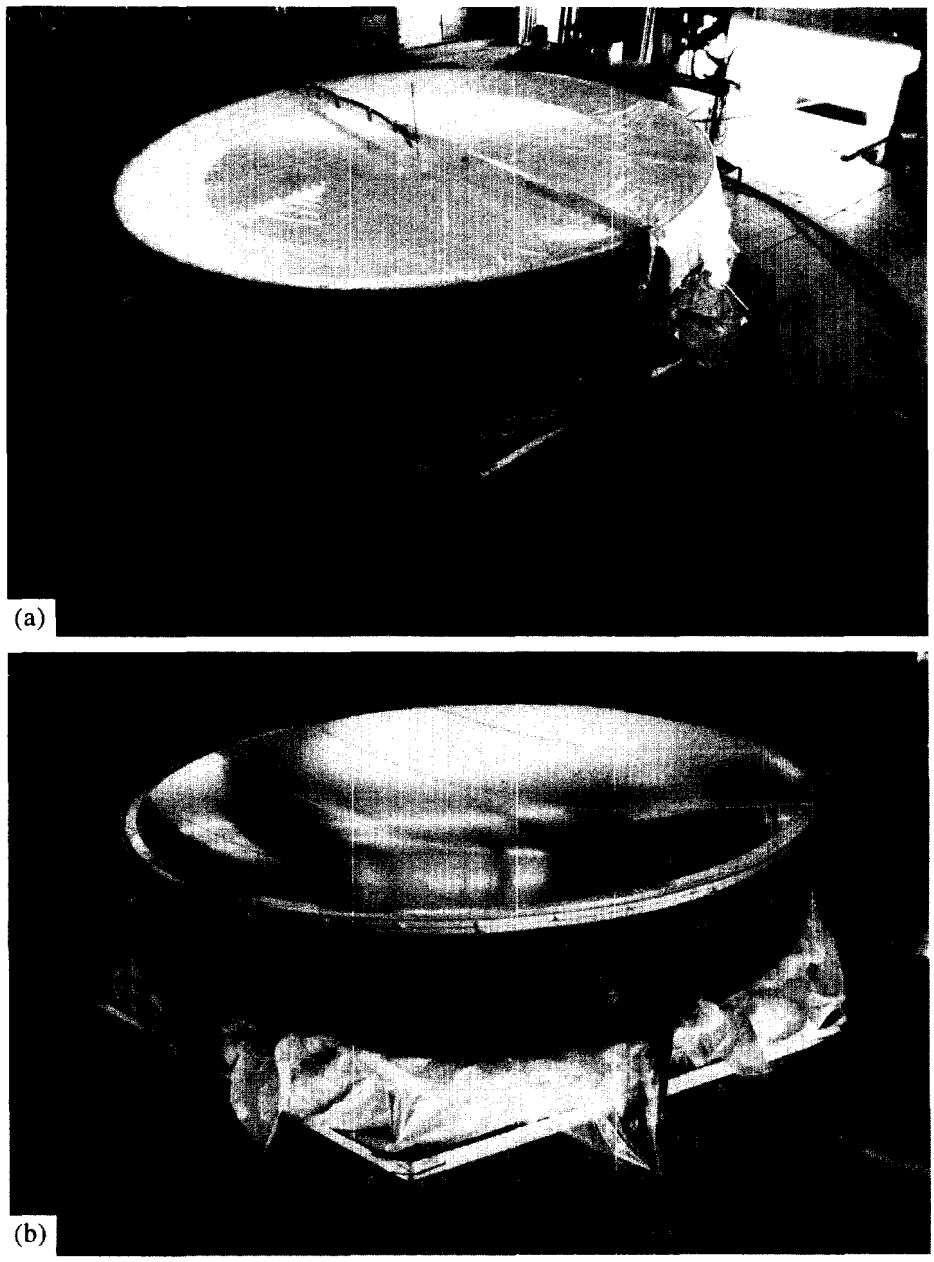

Fig. 8. (a) Forming experiment using hydrostatic pressure; (b) a plastically formed stainless steel test membrane.

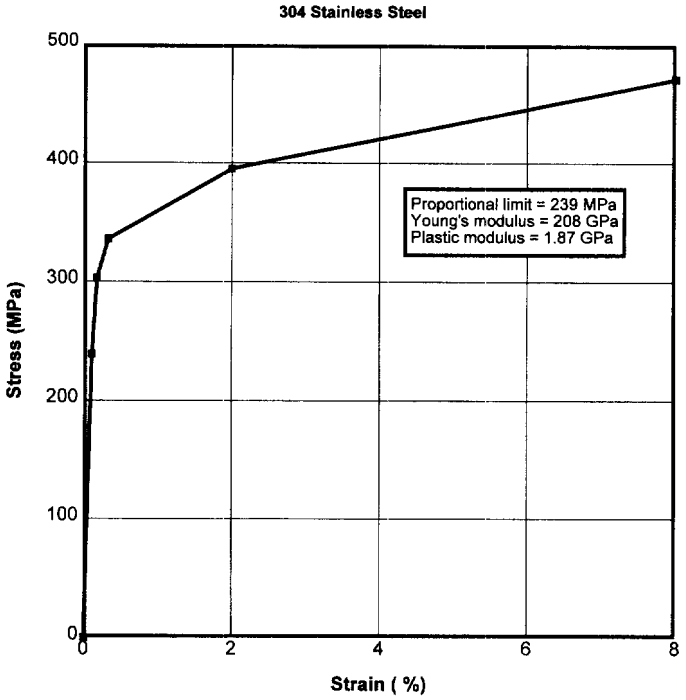

Fig. 9. Tensile stress-strain curve for 304 stainless steel.

Table 3. Comparison of results

Load step	1	2	3	4	5	6	7	8	9	10
Vacuum (Pa)	0.0	684.0	1867.0	3485.0	3858.0	5290.0	5538.0	7094.0	7219.0	7592.0
V (m^3)	0.341	0.491	0.791	1.198	1.332	1.636	1.696	1.959	2.032	2.167
	(0.330)	(0.445)	(0.788)	(1.216)	(1.307)	(1.628)	(1.680)	(1.986)	(2.011)	(2.126)
W_o (cm)	6.31	9.08	14.60	22.13	24.60	30.20	31.30	36.18	37.52	39.99
	(6.59)	(8.45)	(15.03)	(22.83)	(24.48)	(30.22)	(31.13)	(36.44)	(36.85)	(38.11)
Slope @ $r = a$	3.88	5.58	8.94	13.40	14.83	18.01	18.64	21.28	21.99	23.32
(deg.)	(3.12)	(4.85)	(8.39)	(12.94)	(13.89)	(17.24)	(17.78)	(20.86)	(21.12)	(21.95)
σ_r @ $r = a$	166.0	424.0	605.0	713.0	714.0	787.0	794.0	873.0	863.0	860.0
(MPa)	(140.0)	(260.0)	(334.0)	(372.0)	(379.0)	(403.0)	(407.0)	(431.0)	(432.0)	(435.0)
ε_r @ $r = 0$	1000.0	2000.0	4000.0	9000.0	12000.0	17000.0	19000.0	25000.0	27000.0	30000.0
(micro)	(862.0)	(1546.0)	(5497.0)	(11433)	(12752)	(16987)	(17523)	(20536)	(20694)	(21169)

Note: The tabulated values were test data obtained from membrane forming experiment and ANSYS simulation results are shown in parentheses.

6. CONCLUSIONS

The highly nonlinear problems of ponding on circular membranes have been solved with excellent accuracy by the fourth-order Runge-Kutta numerical integration as well as by finite element simulation.

The elastic horizontal displacement $u(r)$ of the membrane obtained under full ponding load was found to be at least one order of magnitude smaller than the vertical deflection $w(r)$. For membranes under partial ponding loads, the horizontal displacements were even smaller (see Table 2) such that their effect on the membrane deformed shapes was negligible.

Under partial ponding loads, the curvature of the deformed membrane shape shows a discontinuity at the fluid boundary while an inflection point (i.e., zero curvature) forms inside the ponding. This characteristic of membrane ponding problem was also reported by Szyszkowski and Glockner (1984).

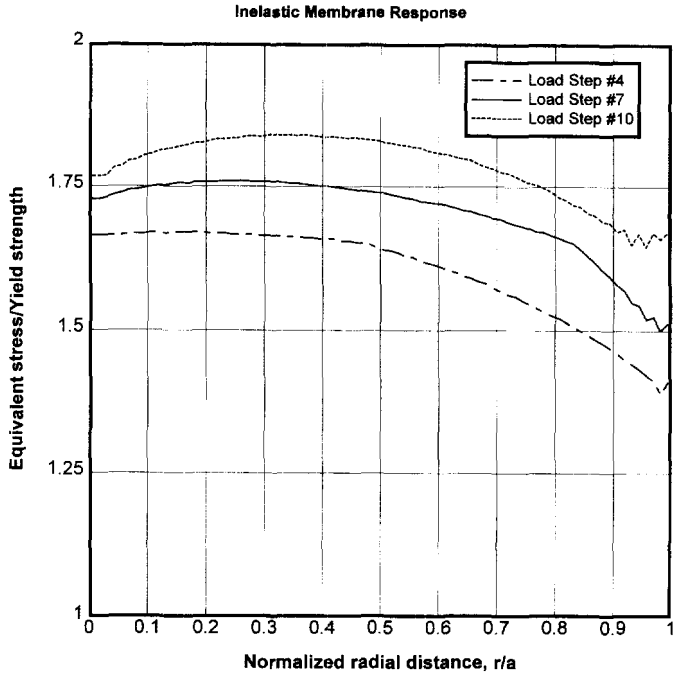

Fig. 10. Equivalent stress distributions for membrane under full ponding.

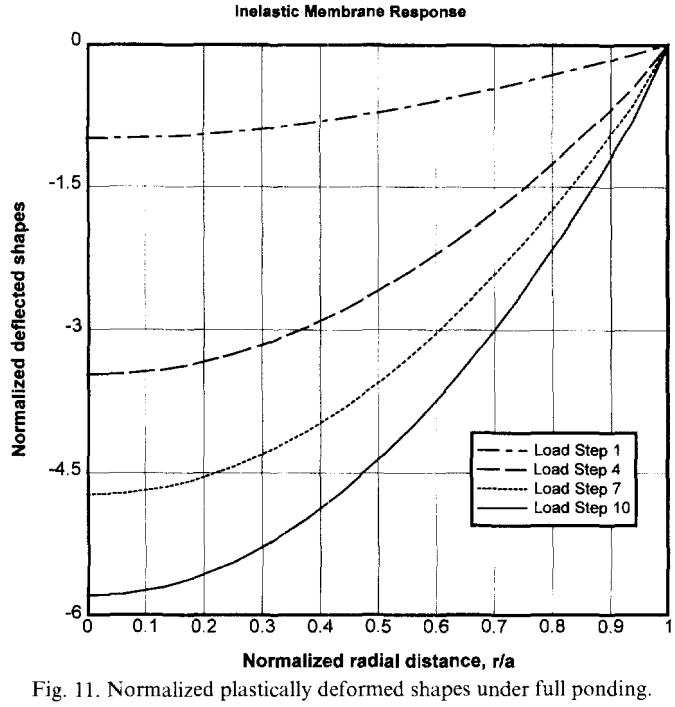

Fig. 11. Normalized plastically deformed shapes under full ponding.

Membranes under partial ponding loads were solved using the same numerical solution algorithm as for full ponding load except with a linear transformation, $w^* = w - w_b$. An iterative finite element solution algorithm using ANSYS code was also developed for the solution to the membrane ponding problems. In the elastic membrane response analyses, the finite element simulation results were virtually identical to those obtained by the fourth-order Runge-Kutta numerical integration (see Table 2). The finite element simulation algorithm was thus proven to be accurate and then used in the simulations of membrane forming experiments where inelastic material response became significant. This numerical

simulation procedure has proven to be very accurate when validated against test data from the membrane forming experiments.

REFERENCES

Epstein, H. I. (1980) Floating roof analysis and design using minicomputers. *Computers and Structures* **11**(4), 349–353.

Epstein, H. I. and Strnad, T. J. (1985) Liquid-filled, liquid-supported circular structural membranes. *Computers and Structures* **21**(3), 443–451.

Kao, R. and Perrone, N. (1971) Large deflections of axisymmetric circular membranes. *International Journal of Solids and Structures* **7**, 1601–1612.

Kelkar, A. *et al.* (1985) Large deflections of circular isotropic membranes subjected to arbitrary axisymmetric loading. *Computers and Structures* **21**(3), 413–421.

Kohnke, P. C. (1993) *ANSYS Theoretical Manual*, Swanson Analysis Systems, Inc., 4.1–4.31.

Mendelson, A. (1968) *Plasticity: Theory and Applications*, Macmillan, New York, U.S.A.

Szyszkowski, W. and Glockner, P. G. (1984) Finite deformation and stability behavior of spherical inflatables subjected to axi-symmetric hydrostatic loading. *International Journal of Solids and Structures* **20**(11/12), 1021–1036.

Timoshenko, S. P. and Woinowsky-Krieger, S. (1959) *Theory of Plates and Shells*, second ed. McGraw-Hill, New York, U.S.A.

Tuan, C. Y. and White, D. L. (1990) Formation of circular optical membranes under free-form yielding. *Journal of Structural Engineering, ASCE* **116**(8), 2299–2308.